



Smooth particle hydrodynamics studies of wet granular column collapses

Guanjin Wang¹ · Amir Riaz¹ · Balakumar Balachandran¹

Received: 13 April 2018 / Accepted: 30 May 2019 / Published online: 11 June 2019
© Springer-Verlag GmbH Germany, part of Springer Nature 2019

Abstract

Dry granular materials have been the subject of many investigations, while wet granular materials, which widely exist in many real-world applications, have only received limited attention. The aim of this paper is to address the missing gap in continuum modeling of wet granular materials. To study the wet granular flows, a grain-scale capillary interaction is introduced, as additional cohesive stress in the continuum-scale framework. We coupled the viscoplastic constitutive law for dry granular material and cohesion model for wet isotropic granular material to capture the behavior of wet granular materials. This combined model is implemented in a smooth particle hydrodynamics framework because the meshfree nature of this method captures the large deformation of granular flows without local grid distortion. The Wendland kernel is used as the interpolation kernel to improve numerical stability. This framework is validated by comparing numerical results with recent experimental findings for both dry and wet cases. The comparisons are illustrative of the potential of the framework to capture the behavior of granular materials across different phases. For different levels of friction and water content, the run-out dynamics and shear strength properties of granular materials in the final quasi-static regime are investigated. For granular flows on flat surfaces, compared with dry granular materials, with the introduction of surface tension in wet granular materials, it is found that there are increases in shear stresses locally and globally, enabling stronger internal forces to support structures with larger angles of repose. The surface energy-induced cohesion is found to play an important role in low friction cases compared to high friction cases. To benchmark the numerical framework presented here, granular column collapses on curved surfaces are also investigated. For flows on curved surfaces, although there are also increases in internal shear stresses, the differences in final profiles between wet granular materials and dry granular materials are not as pronounced as that on flat surfaces due to geometric constraints. The findings of this work are demonstrative of the capabilities of the smooth particle hydrodynamics method for the study of wet granular materials. This effort can serve as a step forward in the quest for a unified continuum theory and computational framework of granular material dynamics.

Keywords Capillary interaction · Cohesive stress · Constitutive modeling · Continuum modeling · Smooth particle hydrodynamics · Wet granular material

1 Introduction

Granular materials are ubiquitous and important as a manipulated industrial material. Fundamentally, granular material problems have multi-physics, multi-scale and multi-phase features. Complex and unique physical

phenomena are often observed with these materials, and these phenomena have evoked the interest of researchers across a range of disciplines. From an application standpoint, granular materials are used in many engineering and commercial applications, for example, agriculture, geo-engineering, pharmaceuticals, and energy production [13, 21]. Most studies on granular media have focused on dry granular materials without consideration of liquid between the grains [3, 15, 22, 26, 35, 38, 40]. However, wet granular materials exist in many real-world problems [1].

✉ Balakumar Balachandran
balab@umd.edu

¹ Department of Mechanical Engineering, University of Maryland, College Park, MD 20742, USA

The major effect that liquid between grains induces is the cohesion in the system. Cohesion in the wet granular system depends on the amount of liquid in the media. As indicated in Fig. 1, the water saturation in wet granular materials may be divided into the following four regimes as described in [28] and [10]:

- Pendular state: Capillary bridges (liquid bridge, pendular ring or meniscus) hold together granular particles when air domain is connected.
- Funicular state: Pores are either fully saturated by liquid or filled with air when pendular rings collapse on one another.
- Capillary state: All pores are filled with liquid when liquid domain is connected.
- Slurry state: Granular particles are immersed in liquid and no capillary interactions at the surface.

A small amount of liquid among grains can have a considerable influence on the mechanical behavior of granular matter. Due to the grain size of particles, thermal noise is omitted in consideration of particle dynamics and the interactions between particles are taken to be dissipative. For dry granular materials, where the interstitial fluids are negligible for the particle motion, the dominant particle interactions are due to friction and collision, which are cohesionless and short range. For wet granular materials, wherein the liquid between grains is considered, the dominant interactions between grains are cohesive due to the surface tension [28]. During the collapse of wet granular material in pendular state (water clinging to soil or sand particles when the moisture content does not reach

specific yield), from experimental evidence, one can infer that due to the introduction of surface tension, the angle of repose is greater than that for a dry sand pile [36, 37, 39, 43].

A continuum constitutive law for granular flow would be helpful for understanding natural processes and for the design and prediction of industrial processes. Through many studies, constitutive frameworks for dry granular materials have been developed for various different geometries and regimes on the basis of theoretical, numerical and experimental efforts. To date, the rheology-based constitutive law provides a unifying framework for dry dense granular flows across steady and non-steady states [5, 16, 17]. However, there is no constitutive relationship for wet granular material in the dense flow regime.

Flow and collapse of granular materials are usually associated with large deformation and plastic failure. Approaches for solving these problems are based on either a discrete point of view or a continuum point of view. The discrete element method (DEM) is an accurate approach for granular material modeling and simulation since this method can be used to capture the discrete nature of the granular system [7, 11, 12, 41]. A drawback of DEM is that it suffers from a high computational cost. Recently, meshfree methods have gained popularity. Unlike the grid-based Eulerian method, the Lagrangian nature of meshfree methods allows one to capture large deformations during granular flow and collapse without local grid distortion. Several researchers have also employed the material point method (MPM) or the smooth particle hydrodynamics (SPH) for modeling and simulation of dry granular






Liquid Content	Saturation Regime	Schematic Diagram	Mean Forces	Physical Description
No	Dry		Gravity, contact	Cohesive stresses between grains are negligible
Small	Pendular		Gravity, contact, capillary	Cohesive forces act through Liquid bridges formed at contact points of grains
Middle	Funicular		Gravity, contact, capillary	Cohesion between particles rises from liquid bridges around the contact points and liquid-filled pores
Almost Saturated	Capillary		Gravity, contact, capillary, [drag]	Cohesive interaction is due to suction, when almost all pores are filled with the liquid. The liquid surface forms menisci and the liquid pressure is lower than the air pressure.
Saturated	Slurry		Gravity, contact, capillary, [drag]	No cohesive interaction exists between particles. The liquid pressure is not lower than the air pressure.

Fig. 1 Granular material saturation states (adapted and revised from [28] and [10])

materials and shown the capability of these methods for studies of granular material systems [2, 4, 6, 9, 14, 18, 20, 23, 27, 29, 31–34, 42, 44]. To date, no SPH-based computational framework has been proposed for wet granular materials.

To extend the use of SPH for studies of wet granular materials, the authors have introduced the concept of capillary interaction as cohesion in the constitutive law of the continuum modeling framework. The proposed framework is validated by comparing the numerical results with recent experimental results. The run-out dynamics at different friction and cohesion levels are then studied. To uncover clues about the underlying mechanisms, the shear strength properties are also examined. To benchmark meshfree models for granular dynamics, the authors have extended the developed SPH framework for dry and wet granular flows over different geometries and topology.

The rest of the paper is organized as follows. In Sect. 2, the authors have discussed the formulation used to model wet granular materials. Subsequently, in Sect. 3, the numerical implementation of the governing equations and boundary conditions in the SPH framework is addressed. In Sect. 4, comparisons are made between numerical results and experimental results available in the literature. Following that, the authors have presented numerical examples to demonstrate the capability of the proposed SPH framework for capturing granular material behavior across different phases and geometric conditions. Finally, in the last section, the authors have collected together the concluding remarks.

2 Governing equations

As granular materials exhibit solid-like behavior, fluid-like behavior and gas-like behavior, the basic governing equations are a combination of the constitutive law in solid mechanics, the conservation laws in fluid mechanics and the equation of state for gas dynamics.

2.1 Physical laws of conservation

Following the standard notation for continuum mechanics, the momentum equation is given by

$$\frac{D\mathbf{v}}{Dt} = \frac{1}{\rho}(\nabla \cdot \boldsymbol{\sigma}) + \mathbf{b} \quad (1)$$

where \mathbf{v} is the velocity vector, ρ is the material density, \mathbf{b} is the specific body force, and $\boldsymbol{\sigma}$ is the Cauchy stress tensor. The total material time derivative is defined as

$$\frac{D(\cdot)}{Dt} = \frac{\partial(\cdot)}{\partial t} + \mathbf{v} \cdot \frac{\partial(\cdot)}{\partial \mathbf{x}} \quad (2)$$

and the spatial velocity gradient has the form

$$\mathbf{L} = \nabla \mathbf{v} \quad (3)$$

The spin rate tensor and strain rate tensor are defined as

$$\mathbf{W} = \frac{1}{2}(\mathbf{L} - \mathbf{L}^T) \quad (4)$$

$$\mathbf{D} = \frac{1}{2}(\mathbf{L} + \mathbf{L}^T) \quad (5)$$

Writing the trace of the tensor \mathbf{L} as $tr\mathbf{L}$, the conservation of mass is described by

$$\frac{D\rho}{Dt} = -\rho tr\mathbf{L} \quad (6)$$

2.2 Constitutive law

A viscoplastic constitutive relationship developed for granular material in dense regime is adopted and revised from earlier work [16] to describe the granular media by the following equation:

$$\boldsymbol{\sigma} = \begin{cases} -P\mathbf{I} + \frac{(\mu P + c)\mathbf{D}}{|\mathbf{D}|} & \text{for } I \geq 0.001 \\ -P\mathbf{I} + (\mu P + c)sign(\mathbf{D}) & \text{for } I < 0.001 \end{cases} \quad (7)$$

Here, the first term in Eq. (7) is the hydro-static pressure, and the second term in Eq. (7) is the deviatoric shear stress, μ is the friction coefficient, P is the pressure, c is representative of cohesion, \mathbf{I} is the identity tensor, I is the inertial number (when $I < 0.001$, the granular material is in quasi-static regime and when $I \geq 0.001$ the granular material is in dense regime from [26]) and $|\mathbf{D}| = \sqrt{\frac{1}{2}\mathbf{D} : \mathbf{D}}$ is the second invariant of the strain rate tensor. To avoid singularities, $|\mathbf{D}| + \epsilon$ is adopted and ϵ is set to 0.01 h^2 in the numerical simulation as suggested in previous work [14]. The pressure is determined by using the equation of state as follows

$$P = \begin{cases} \kappa[(\frac{\rho}{\rho_o})^\gamma - 1](1 + w) & \text{for } \rho > \rho_o \\ 0 & \text{for } \rho \leq \rho_o \end{cases} \quad (8)$$

wherein ρ_o is the reference density, κ is related to the bulk modulus and set to 28,000, w is the gravimetric water content (the ratio between the weight of water and the weight of the dry granular particles), γ is a scaling parameter and set to 7 as suggested in the literature [42]. The friction law follows from reference [5, 16] and reads as

$$\mu(I) = \mu_1 + \frac{\mu_2 - \mu_1}{I_0/I + 1} \tag{9}$$

where μ_1 is the friction coefficient for the quasi-static limit, μ_2 is a limiting coefficient for granular material in the dynamic flow regime, and I is the inertia number defined as

$$I = \frac{|\mathbf{D}|d}{\sqrt{P/\rho_s}} \tag{10}$$

Here, d is the grain diameter and set to 2 mm for all the simulations and ρ_s is the particle density. For dry cohesionless particles, c is set to 0. For wet granular particles in the pendular state, the cohesion arises from surface tension and capillary strengthening effects. Rumpf [19] estimated cohesive stress for isotropic granular material with identical diameters as

$$c = \frac{vkF}{\pi d^2} \tag{11}$$

where v is the grain packing fraction. For all the wet granular material simulations in this paper, k is assumed to be 6 according to experimental results from [36] and [37], which is the average number for the liquid bridge between a pair of particles, and F is the average force per liquid bridge that is given by

$$F = \frac{2\pi r\gamma_s}{1 + \tan(\varphi/2)} \tag{12}$$

where r is the grain radius, γ_s is the surface tension, and φ is defined in Fig. 2. Note that the particles in Fig. 2 are not SPH particles but real granular material particles. In the simulation, parameters are taken from physical experiments [11].

3 Numerical implementation

3.1 The SPH method

Smooth particle hydrodynamics is a meshfree Lagrangian method. As with other discretization approaches, in the SPH method, the solution domain is first discretized and represented by a certain number of particles [4, 29]. Thus,

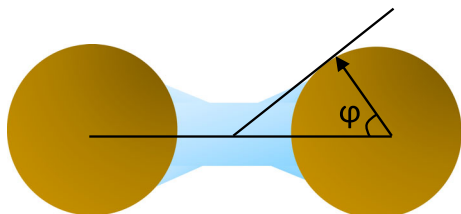


Fig. 2 Illustration of liquid bridge between two granular material particles

all the field properties, such as density, velocity, and strain rate, are carried by these SPH particles. The properties of the particles of interest are then interpolated over their neighboring particles by using an approximation function, called the kernel function, which is usually represented by W (see Fig. 3). Although the most popular B-spline kernel function often yields a good balance between accuracy and stability, the Wendland kernel function is adopted from [8] in this work to provide robust and stable solutions without using artificial stress method [30]. This function takes the following form:

$$W_{ij} = \alpha_d \times \begin{cases} \left(1 - \frac{q}{2}\right)^4 (2q + 1) & \text{for } q \leq 2 \\ 0 & \text{otherwise} \end{cases} \tag{13}$$

Here, for two-dimensional and three-dimensional problems, α_d is set to $7/(4\pi h^2)$ and $21/(16\pi h^3)$, respectively, $q = r/h$, r is the distance between two particles, and h is the smoothing length. Then, the particle approximation/interpolation for any field quantity $f(x)$ and its derivatives at point i can be expressed as

$$f(\mathbf{x}_i) = \sum_{j=1}^N \frac{m_j}{\rho_j} f(\mathbf{x}_j) W_{ij} \tag{14}$$

$$\nabla f(\mathbf{x}_i) = \sum_{j=1}^N \frac{m_j}{\rho_j} f(\mathbf{x}_j) \nabla_i W_{ij} \tag{15}$$

where $W_{ij} = W(\mathbf{r}_{ij}, h)$ and

$$\nabla_i W_{ij} = \frac{\mathbf{x}_i - \mathbf{x}_j}{r_{ij}} \frac{\partial W_{ij}}{\partial r_{ij}} \tag{16}$$

3.2 SPH for granular flow

Summation density: Two approaches to evolve density are adopted in the SPH framework. For density initialization of a particle i , the density calculated by using the summation density approach is written as

$$\rho_i = \sum_j m_j W_{ij} \tag{17}$$

For density re-initialization, the Shepard filter is applied every 10 time steps to reduce the inaccuracies near the boundaries and free surfaces; this is given by

$$\rho_i = \frac{\sum_j m_j W_{ij}}{\sum_j \frac{m_j}{\rho_j} W_{ij}} \tag{18}$$

Continuity density: For density evolution at each time step, the continuity density is calculated from the continuity equation. The δ SPH scheme is adopted from reference

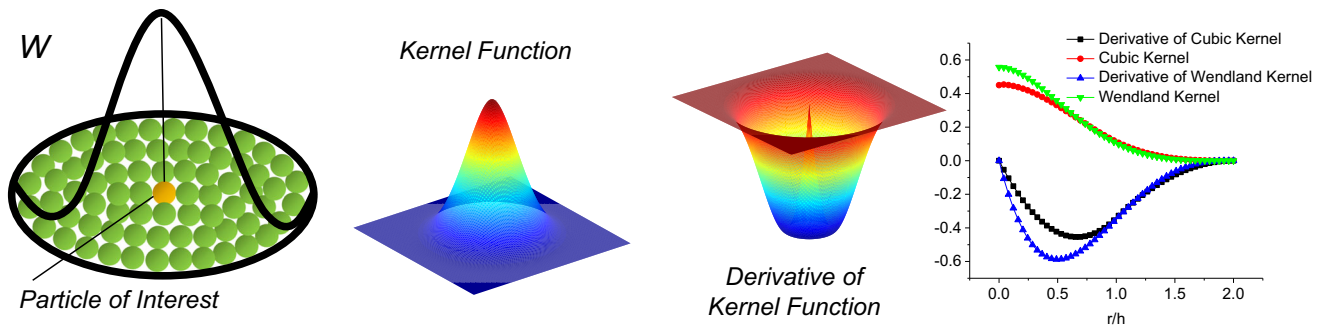


Fig. 3 Kernel function

[25] to reduce high-frequency oscillations by introducing a diffusive term that takes the form

$$\frac{D\rho_i}{Dt} = \sum_j m_j (\mathbf{v}_i - \mathbf{v}_j) \cdot \nabla_i \mathbf{W}_{ij} + \sum_j \psi_{ij} \mathbf{r}_{ij} \nabla_i \mathbf{W}_{ij} \quad (19)$$

where ψ_{ij} is defined as

$$\psi_{ij} = \frac{2\delta hc_o(\rho_j - \rho_i)m_j}{\rho_j |\mathbf{r}_{ij}^2|} \quad (20)$$

Here, δ is set to 0.01, c_o is the artificial sound speed set as

$$c_o = \sqrt{\frac{\kappa\gamma\rho_s}{\rho_o(\rho_s - \rho_o)}} \quad (21)$$

Particle approximation of momentum: To reduce errors associated with particle inconsistencies, the momentum equation is approximated as

$$\frac{D\mathbf{v}_i}{Dt} = \sum_j m_j \left(\frac{\boldsymbol{\sigma}_i}{\rho_i^2} + \frac{\boldsymbol{\sigma}_j}{\rho_j^2} - \Pi_{ij} \right) \cdot \nabla_i \mathbf{W}_{ij} + \mathbf{b} \quad (22)$$

where \mathbf{b} is the body force. The quantity Π is the artificial viscosity adopted to improve numerical stability and avoid inter-particle penetration. This quantity is formulated as

$$\Pi_{ij} = \begin{cases} \frac{-\alpha_{\Pi} c_{ij} \phi_{ij} + \beta_{\Pi} \phi_{ij}^2}{\rho_{ij}} & \text{for } \mathbf{v}_{ij} \cdot \mathbf{x}_{ij} < 0 \\ 0 & \text{for } 0 \leq \mathbf{v}_{ij} \cdot \mathbf{x}_{ij} \end{cases} \quad (23)$$

$$\phi_{ij} = \frac{h_{ij} \mathbf{v}_{ij} \cdot \mathbf{x}_{ij}}{|\mathbf{x}_{ij}|^2 + 0.01 h_{ij}^2} \quad (24)$$

Here, $c_{ij} = (c_i + c_j)/2$, here both c_i and c_j are set to c_o as defined in Eq. (21), $\rho_{ij} = (\rho_i + \rho_j)/2$, $h_{ij} = (h_i + h_j)/2$, and $\mathbf{x}_{ij} = \mathbf{x}_i - \mathbf{x}_j$, $\mathbf{v}_{ij} = \mathbf{v}_i - \mathbf{v}_j$. c is computed through Eq. (21), α_{Π} is set to 1 and β_{Π} is set to 0 as the second quadratic term in the artificial viscosity is used to handle high Mach number flows [24]. To evaluate the stress tensor in Eq. (22), the velocity gradient needs to be interpolated as follows

$$\nabla \mathbf{v}_i = \sum_j \frac{m_j}{\rho_j} (\mathbf{v}_j - \mathbf{v}_i) \otimes \nabla_i \mathbf{W}_{ij} \quad (25)$$

The extended smoothed particle hydrodynamics (XSPH) is employed from prior work [29] to stabilize particles at free surfaces and avoid unphysical penetration. This is given by

$$\frac{d\mathbf{r}_i}{dt} = \mathbf{v}_i + \chi \sum_j \frac{m_j}{\rho_{ij}} (\mathbf{v}_j - \mathbf{v}_i) W_{ij} \quad (26)$$

where χ is set to 0.2.

3.3 Boundary conditions

Two types of boundary conditions are employed in this research. The first is the solid boundary wall. To generate a solid boundary, the stress tensor for solid boundary particles is calculated by using Eq. (7). Also, ghost particles are used to remove the boundary inaccuracies in SPH methods. The velocity and stress for the ghost particles are set in accordance with earlier work [2].

3.4 Integration

For integrating the Newton’s law of motion, the popular Verlet–Leapfrog algorithm is used. In adopting this approach, the field variables such as density, velocity vectors, and position vectors are updated at every time step as follows:

$$\rho_i^{n+1/2} = \rho_i^{n-1/2} + \Delta t \frac{D\rho_i^n}{Dt} \quad (27)$$

$$\mathbf{v}_i^{n+1/2} = \mathbf{v}_i^n + \frac{\Delta t}{2} \frac{D\mathbf{v}_i^n}{Dt} \quad (28)$$

$$\mathbf{r}_i^{n+1/2} = \mathbf{r}_i^n + \Delta t \mathbf{v}_i^{n+1/2} \quad (29)$$

The Courant–Friedrichs–Lewy condition is used to determine the time step to satisfy the following:

$$\Delta t \leq C_{\text{cour}} \left(\frac{h}{c_s} \right) \quad (30)$$

Here, h is the smoothing length, c_s is the sound speed calculated by Eq. (21), and C_{cour} is the Courant coefficient.

4 Results and discussion

The granular column collapse case is employed to test the rheology-based constitutive relationship used for wet granular materials. It is shown that the results generated from the current constitutive law are consistent with experimental findings for both dry and wet cases, as illustrated in Fig. 4. The parameters μ_1 and μ_2 correspond approximately to parameters of glass beads in [16] are used in the implementation of the friction law Eq. (9) for both the dry granular media and wet granular media studies. (The full list of parameters are shown in Table 1 consistent with [11]). In Fig. 4a, two typical final configurations of wet and dry granular column collapse are shown from [11]. In Fig. 4b, the qualitative results of two typical simulations of wet and dry granular column collapses are shown, which

is similar to the experimental findings in [11]. It is evident that larger cohesion in wet granular column collapses gives rise to a shorter run-out length and larger angles of repose. In Fig. 4c, k is assumed to be 6 for all the wet granular material simulations, according to experimental results from [36] and [37]. The grain diameter d is 0.002m. The final profiles are shown with the increase in liquid content. In the simulations, the results of the influence of liquid content on the final profiles are similar to experimental findings. Dry and wet conditions seem distinct, while differences between wet cases seem smaller. Having verified that the proposed SPH formulation can be used for dry granular media and wet granular media studies, the authors then consider other illustrative cases.

Next, the authors consider transient and steady-state phenomena and associated characteristics related to particle dynamics during granular column collapses, such as run-out distance, the angle of repose, strain developed during the collapse. The shear strength properties are also studied to uncover clues related to the underlying mechanisms during the collapse.

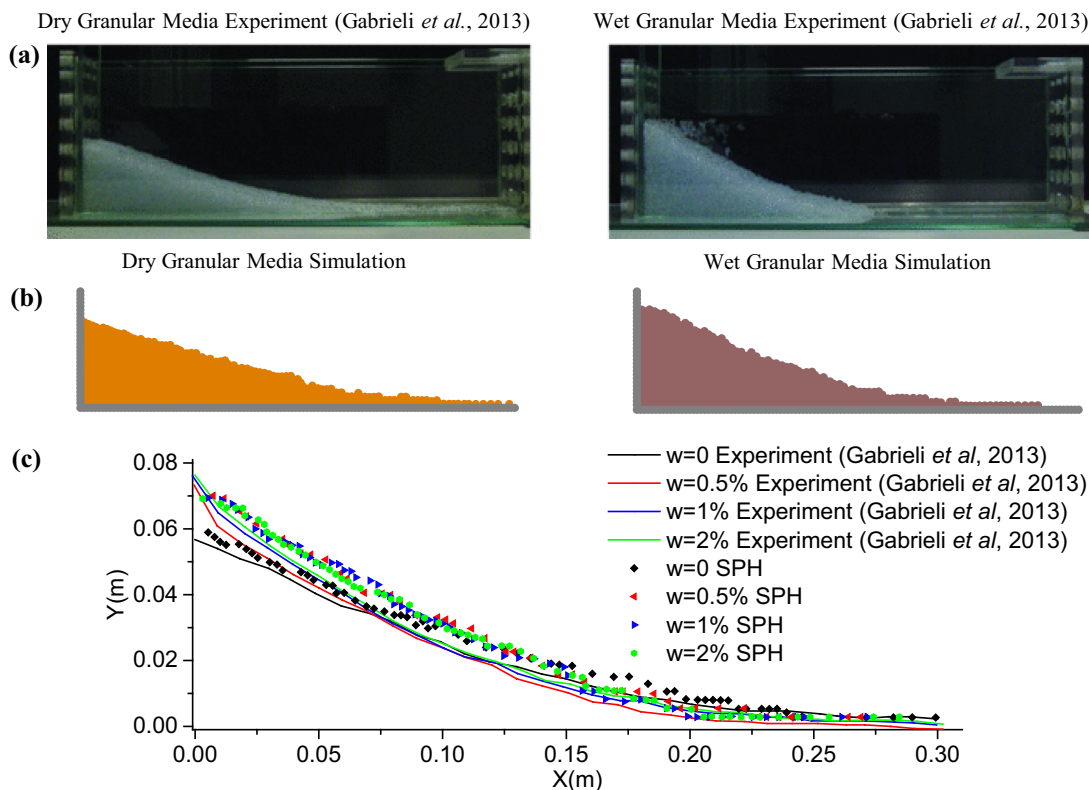


Fig. 4 Validation of final profiles for $d = 2$ mm. **a** Experimental results from the literature [11]. **b** Computational results obtained in the current work for dry and wet conditions: dry granular media simulation ($\mu_1 = \tan(21^\circ)$, $\mu_2 = \tan(33^\circ)$, $w = 0$) and wet granular media simulation ($\mu_1 = \tan(21^\circ)$, $\mu_2 = \tan(33^\circ)$, $w = 0.5\%$). **c** Simulated and experimental final profiles for different water content

Table 1 Parameters used in simulations of the dry granular column and wet granular column collapse

Simulation	ρ_s (kg/m ³)	ρ_o (kg/m ³)	μ_1	μ_2	k	I_o	Δx (m)	γ_s (mN/m)	d (m)	φ
Dry	2532	2507	$\tan(21^\circ)$	$\tan(33^\circ)$	0	0.3	0.0026	0	0.002	0
Wet	$2532 * (1 + w)$	$2507 * (1 + w)$	$\tan(21^\circ)$	$\tan(33^\circ)$	6	0.3	0.0026	72.5	0.002	15°

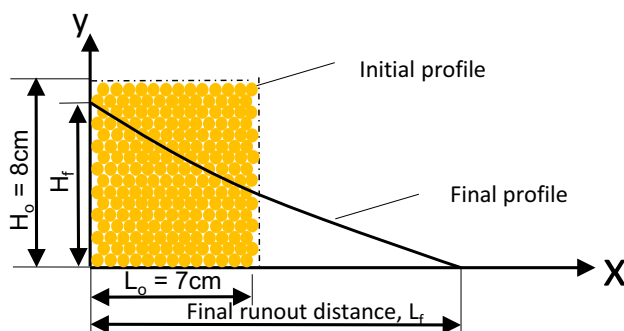
4.1 Run-out dynamics of granular column collapse on flat surfaces

The geometry of the quasi-2D initial configuration ($7 \times 8 \text{ cm}^2$) and surface profile of the final configuration of the granular column is shown in Fig. 5. The particles are aligned in a particular arrangement layer by layer. For all of the numerical results shown for dry and wet granular materials studied in this paper, the parameter values are set to be the same as what is shown in Fig. 4.

The influence of wetting fluid on the run-out dynamics of wet and dry granular column collapse is shown in Fig. 6. It is evident that a small amount of fluid between granular particles impacts the deposit as well as the final shape of the run-out dynamics. In Fig. 6a, the representative profiles of low friction, dry and wet granular materials at different time instants are presented. At $t = 0.01 \text{ s}$, the collapse is triggered and the material starts to flow under gravity; At $t = 0.2 \text{ s}$, the collapse is well developed, the material near the boundary is in the quasi-static regime and the material near the surface is in the dynamic flow regime. At $t = 0.4 \text{ s}$, the occurrence of jamming due to friction at the boundary prevents further collapse. By $t = 0.6 \text{ s}$, one can infer that the internal stresses are quite well distributed and appear to be in a quasi-steady state, particularly in regions close to the boundary and the surface. It is observed that the wet granular material has a shorter run-out distance compared to dry granular material. In Fig. 6b, the horizontal velocity contours are presented for dry and wet granular material at different time instants. It is clear that the wet granular

column collapses more slowly than in the dry case because of the surface tension-induced cohesive stress. In Fig. 6c, the strain developed during the collapse is shown. The wet granular material is noted to deform less than the dry granular material at all representative time instants due to the presence of cohesion. The low level of deformation of wet granular materials leads to a shorter run-out distance and higher final height. In Fig. 6d, final profiles of dry and wet granular columns for different resolutions are shown. The number of interior SPH particles are 475, 1036, and 2310 accordingly for the coarsest resolution, the fit resolution and the finest resolution. The fit resolution is used in other simulations in this paper, since both the results generated using the finest and fit resolution agree with the experimental findings from [11].

In Fig. 7a, steady-state profiles of granular materials are shown for different water content and friction levels ($\mu_1 = \tan(21^\circ)$, $\mu_2 = \tan(33^\circ)$; $\mu_1 = \tan(32^\circ)$, $\mu_2 = \tan(33^\circ)$; $\mu_1 = \tan(32^\circ)$, $\mu_2 = \tan(45^\circ)$). For low frictional granular materials, dry and wet conditions seem distinct, while differences between wet cases of different water content seem smaller. For high frictional granular materials, differences between wet and dry cases are small. In the pendular state, the final profile of the wet granular materials depends on both the water content and friction levels. The differences in water content play a more prominent role in low friction granular materials compared with high friction granular materials. In Fig. 7b, front advancement (normalized run-out distance) during granular column collapses at different time instants is displayed. It is shown that the granular materials reach steady state before 0.6s. The run-out distance is rescaled and non-dimensionalized by $L^* = (L - L_o)/L_o$, where L_o is the initial length of the granular column, and L is the run-out distance of each state. In Fig. 7c, the final normalized run-out distance is plotted for different friction and water content levels. L_f is the run-out distance of the final state. The increase in water content has a strong influence on the final run-out distance when the water content is less than 1%, and small effect when the water content is larger than 1%. In Fig. 7d, the normalized run-out distance is plotted with respect to a dimensionless number as a function of Bond number $Bo = \rho g R^2 / \gamma$, which is the ratio between the body force and capillary force, and

**Fig. 5** Initial geometry and final geometry of granular column

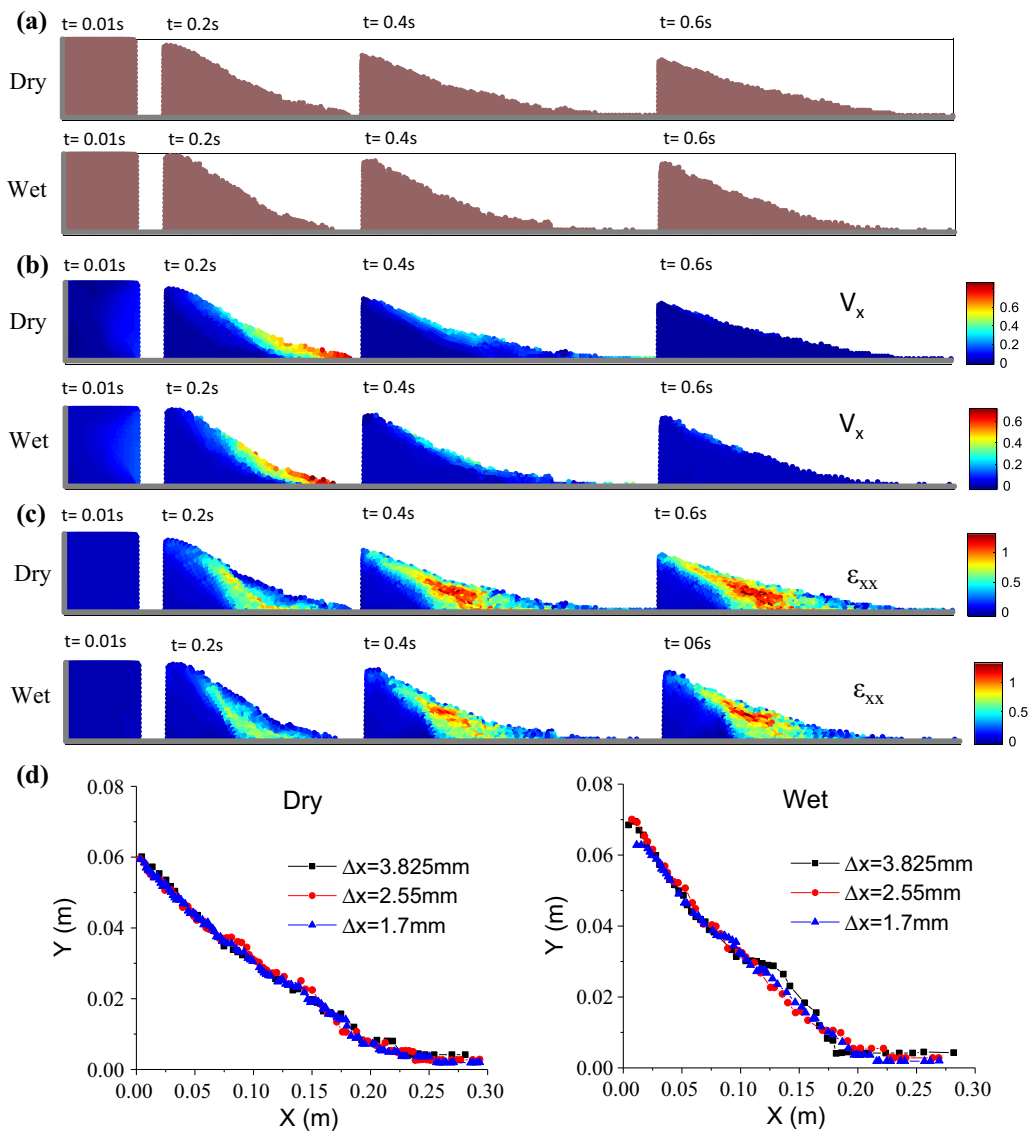


Fig. 6 Run-out dynamics during the collapse of dry granular material ($\mu_1 = \tan(21^\circ)$, $\mu_2 = \tan(33^\circ)$, $w = 0$) and wet granular material ($\mu_1 = \tan(21^\circ)$, $\mu_2 = \tan(33^\circ)$, $w = 0.5\%$). **a** Profiles of dry and wet granular materials at different time instants. **b** Velocity profiles of dry and wet granular materials at different time instants. **c** Strain developed during the collapse of dry and wet granular columns at different time instants. **d** Final profiles with different resolution

the water content w . In Fig. 7e, the final normalized height is plotted for different friction levels and water contents. H_f is the height of the final state. The final height is rescaled and non-dimensionalized by $H^* = H_f/H_o$, where H_o is the initial height of the granular column. In Fig. 7f, the authors plot the absolute value of the maximum shear stress in the material along the pressure isobar for different friction levels of dry and wet granular materials. The yield τ - p loci are plotted and the relationship is close to a straight line, which is in agreement with the Drucker–Prager model as the granular material is in quasi-static regime. It is shown that, in the pendular state, the introduction of capillary

force increases the shear strength which in turn enables a stronger granular structure.

4.2 Gravity-driven granular flow on curved surfaces

Although the primary driving force for a landslide or landslide-like phenomenon is gravity, other contributing factors affect the slope stability. To simulate granular flows across nature-like surfaces and benchmark the authors' numerical model for wet granular material, wet granular flows across different topology and geometry conditions are presented, ranging from circular surfaces to ellipsoidal

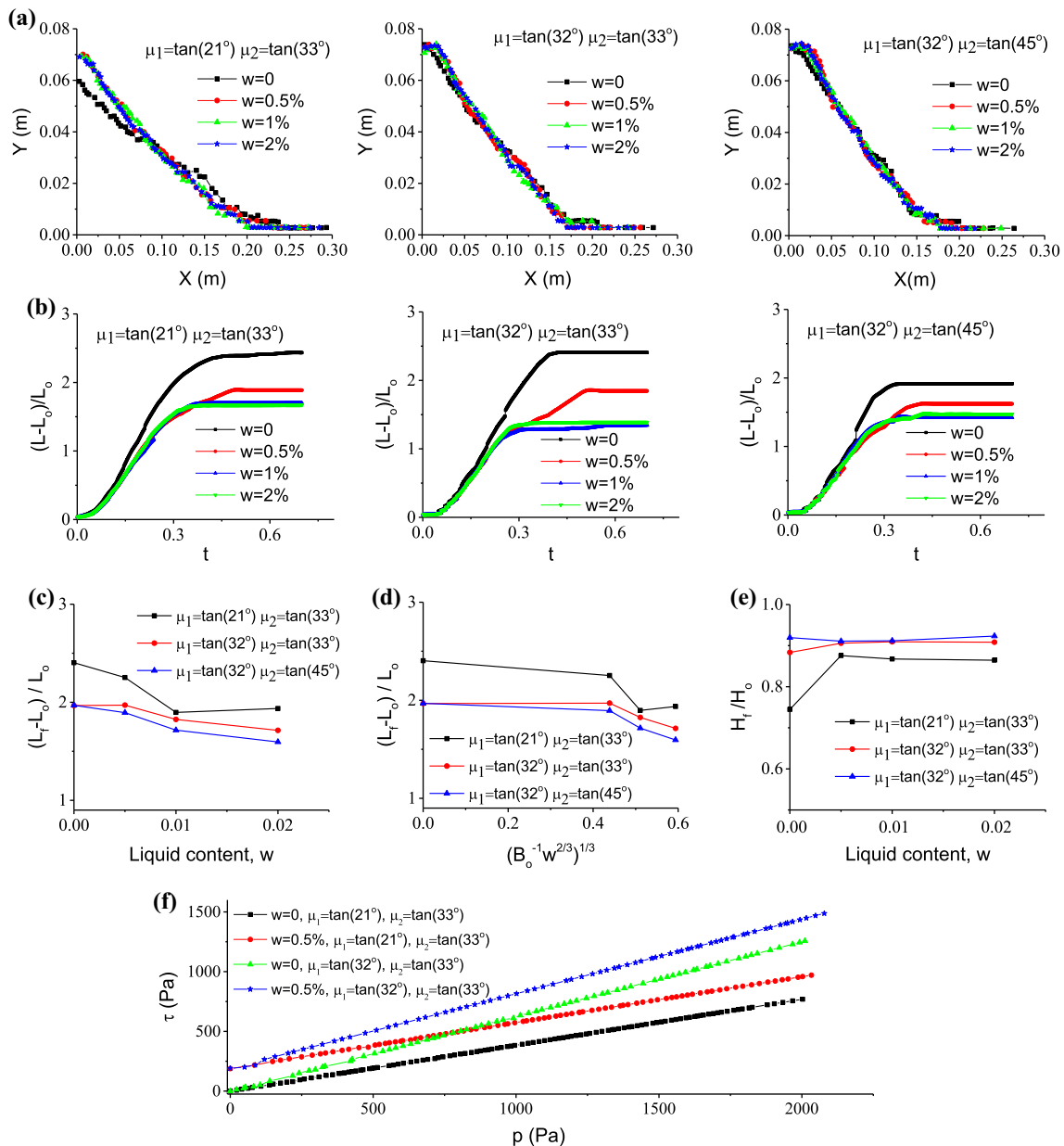


Fig. 7 Parametric study of dry and wet granular column collapses on flat surfaces. **a** Final profiles of granular materials for different friction levels and water contents. **b** Normalized run-out length during granular column collapses for different friction levels and water contents. **c** Normalized final run-out length for different friction levels and water contents. **d** Normalized final run-out length vs dimensionless number $Bo^{-1} w^{2/3}$ for different water content. **e** Normalized final height for different friction levels and water contents. **f** Yield loci τ - σ of dry and wet granular materials in the final state

surfaces. The influence of wetting fluid on the run-out dynamics of wet and dry granular column collapses on curved surfaces is shown in Figs. 8 and 9. For collapses of granular columns on curved surfaces, what is similar to collapses of granular column on flat surfaces is that: in Figs. 8a and 9a, the representative profiles of low friction, dry and wet granular materials at different time instants are presented. Wet granular materials deform less than dry granular materials at all time instants during the collapses.

In Figs. 8b and 9b, the velocity contours are presented for dry and wet granular materials at different time instants. Wet granular column collapses more slowly than dry granular columns because of the surface tension-induced cohesion. In Figs. 8c and 9c, steady-state granular profiles are shown for different levels of water content and friction. In Figs. 8d and 9d, the yield τ - p loci for dry and wet granular materials are plotted and the relationship is close to a straight line, which is in agreement with the Drucker–

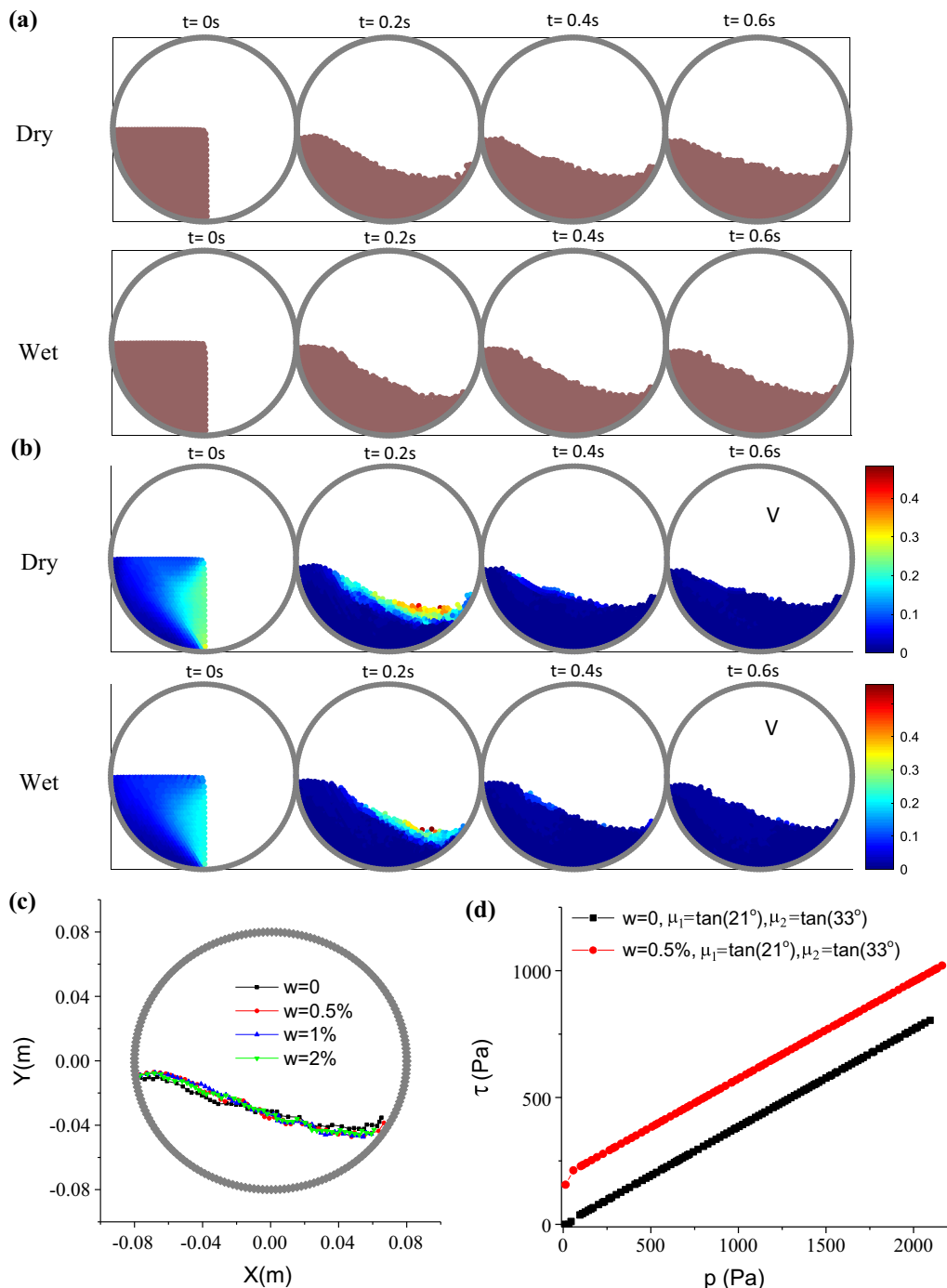


Fig. 8 Granular flows on circular surfaces for $d = 0.002$ m. **a** Profiles of dry granular material ($\mu_1 = \tan(21^\circ)$, $\mu_2 = \tan(33^\circ)$, $w = 0$) and wet granular material ($\mu_1 = \tan(21^\circ)$, $\mu_2 = \tan(33^\circ)$, $w = 0.5\%$) on circular surfaces at different time instants. **b** Velocity profiles of dry granular material and wet granular material on circular surfaces at different time instants. **c** Final profiles of granular material on circular surfaces for different water contents. **d** Yield loci τ - σ of granular flows on circular surfaces in the final state

Prager model as the granular material is in quasi-static regime. It is shown that, in the pendular state, the introduction of capillary force increases the shear strength that make the entire granular structure deform less. However, for granular column collapses on curved surfaces, although the introduction of capillary force increases the shear

strength, the differences in final profiles between wet granular materials and dry granular materials are not as pronounced as that on flat surfaces due to geometric constraints. The geometric constraints of circular and ellipsoidal surfaces hinder the further deformation of granular columns. For collapses on ellipses surfaces, dry and wet

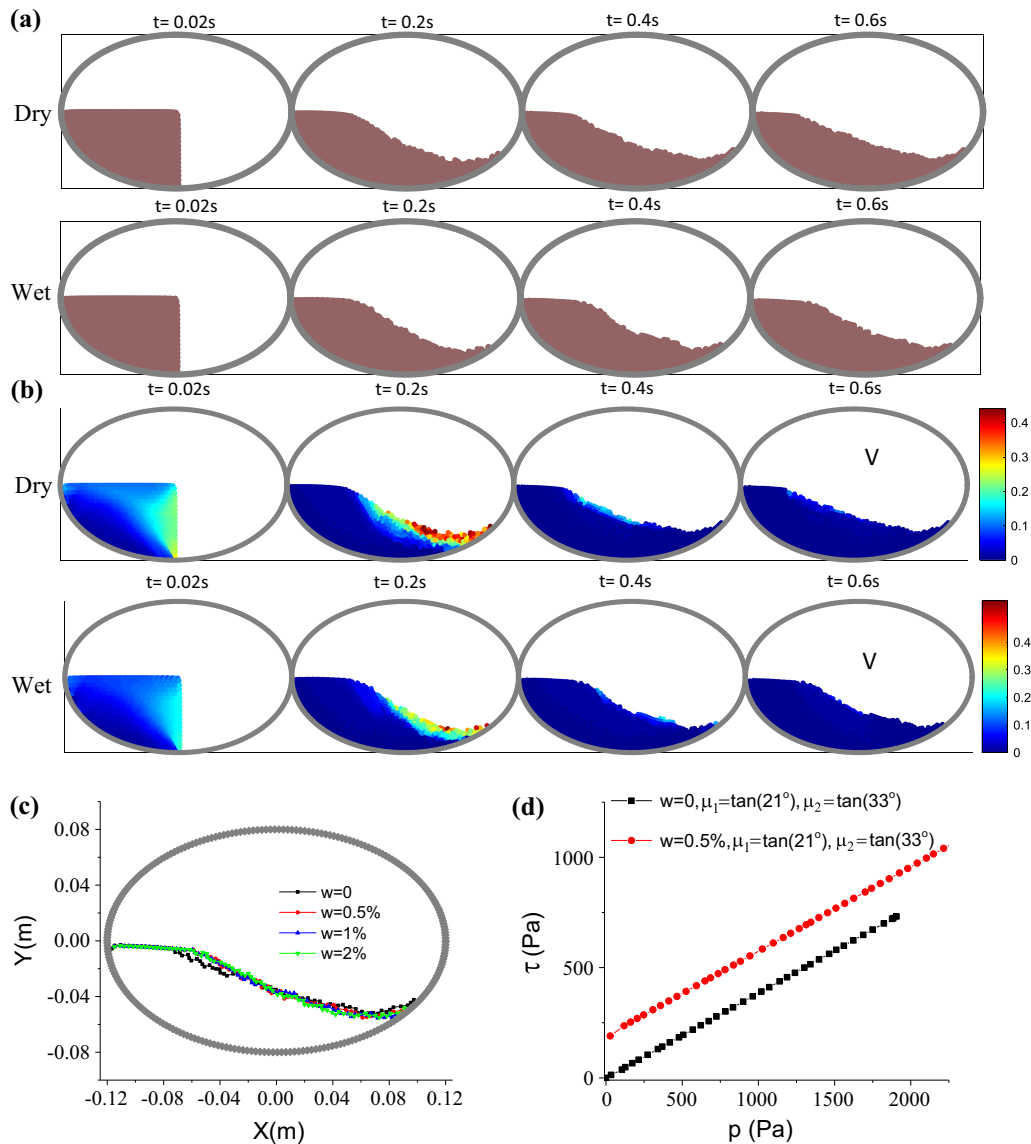


Fig. 9 Granular flows on ellipsoidal surfaces for $d = 0.002$ m. **a** Profiles of dry granular material ($\mu_1 = \tan(21^\circ)$, $\mu_2 = \tan(33^\circ)$, $w = 0$) and wet granular material ($\mu_1 = \tan(21^\circ)$, $\mu_2 = \tan(33^\circ)$, $w = 0.5\%$) on ellipsoidal surfaces at different time instants. **b** Velocity profiles of dry granular material and wet granular material on ellipsoidal surfaces at different time instants. **c** Final profiles of granular material on ellipsoidal surfaces for different water contents. **d** Yield loci τ - σ of granular flows on ellipsoidal surfaces in the final state

conditions seemed more distinct than those on circular surfaces. This indicates the smaller the curvature of the surface is, the more distinct the differences between dry and wet conditions will be.

5 Concluding remarks

A constitutive model for both the dry and wet granular materials is implemented in a smooth particle hydrodynamics framework to investigate the collapse of granular columns on flat and curved surfaces. The grain-scale capillary interaction is taken into consideration for capturing the

behavior of wet granular materials. The proposed SPH framework is validated by comparing numerical results obtained with this model with recent experimental findings for dry and wet granular column collapses on flat surfaces. Compared with dry granular materials, the introduction of surface tension in wet granular materials is noted to increase the shear stresses and enable a stronger structure with larger angles of repose. Although we did not find experimental validation for the simulations of collapses on curved surfaces, future experimental studies may find our results useful to compare with. For collapses on curved surfaces, the differences in final profiles between wet granular materials and dry granular materials are not as pronounced as that on flat

surfaces due to geometric constraints, although there is also an increase in internal shear strength. Through the current study, it is shown that the smooth particle hydrodynamics method can be used to study wet granular materials. In future studies, the authors plan to focus on how to transfer information at the micro-scale to the continuum-scale model to bridge the gap between length scales. Also, implement more reliable cohesion models and size-dependent models in the numerical framework.

Acknowledgements The authors would like to thank the reviewers for the many constructive suggestions provided during the review process. Support received for this work through US National Science Foundation Grant No.1507612 is gratefully acknowledged.

References

- Artoni R, Santomaso AC, Gabrieli F, Tono D, Cola S (2013) Collapse of quasi-two-dimensional wet granular columns. *Phys Rev E* 87(3):032205
- Bui HH, Fukagawa R, Sako K, Ohno S (2008) Lagrangian meshfree particles method (SPH) for large deformation and failure flows of geomaterial using elastic–plastic soil constitutive model. *Int J Numer Anal Methods Geomech* 32(12):1537–1570
- Campbell CS (1990) Rapid granular flows. *Annu Rev Fluid Mech* 22(1):57–90
- Chabalko C, Balachandran B (2013) GPU based simulation of physical systems characterized by mobile discrete interactions. In: Topping BHV, Ivanyi P (eds) *Developments in parallel, distributed, grid, and cloud computing in engineering*. Saxe-Coburg Publications, pp 95–124
- Chambon G, Bouvarel R, Laigle D, Naaim M (2011) Numerical simulations of granular free-surface flows using smoothed particle hydrodynamics. *J Non-Newton Fluid Mech* 166(12–13):698–712
- Chen W, Qiu T (2011) Numerical simulations for large deformation of granular materials using smoothed particle hydrodynamics method. *Int J Geomech* 12(2):127–135
- Da Cruz F, Emam S, Prochnow M, Roux JN, Chevoir F (2005) Rheophysics of dense granular materials: discrete simulation of plane shear flows. *Phys Rev E* 72(2):021309
- Dehnen W, Aly H (2012) Improving convergence in smoothed particle hydrodynamics simulations without pairing instability. *Mon Not R Astron Soc* 425(2):1068–1082
- Dunatunga S (2015) Simulation of granular flows through their many phases. In: *APS meeting abstracts*
- Gabrieli F, Lambert P, Cola S, Calvetti F (2012) Micromechanical modelling of erosion due to evaporation in a partially wet granular slope. *Int J Numer Anal Methods Geomech* 36(7):918–943
- Gabrieli F, Artoni R, Santomaso A, Cola S (2013) Discrete particle simulations and experiments on the collapse of wet granular columns. *Phys Fluids* 25(10):103303
- Guo N, Zhao J (2014) A coupled FEM/DEM approach for hierarchical multiscale modelling of granular media. *Int J Numer Methods Eng* 99(11):789–818
- Henann DL, Kamrin K (2013) A predictive, size-dependent continuum model for dense granular flows. *Proc Natl Acad Sci* 110(17):6730–6735
- Hurley RC, Andrade JE (2017) Continuum modeling of rate-dependent granular flows in SPH. *Comput Part Mech* 4(1):119–130
- Ionescu IR, Mangeney A, Bouchut F, Roche O (2015) Viscoplastic modeling of granular column collapse with pressure-dependent rheology. *J Non-Newton Fluid Mech* 219:1–18
- Jop P, Forterre Y, Pouliquen O (2006) A constitutive law for dense granular flows. *Nature* 441(7094):727
- Kamrin K, Koval G (2012) Nonlocal constitutive relation for steady granular flow. *Phys Rev Lett* 108(17):178301
- Kermani E, Qiu T (2018) Simulation of quasi-static axisymmetric collapse of granular columns using smoothed particle hydrodynamics and discrete element methods. *Acta Geotech*. <https://doi.org/10.1007/s11440-018-0707-9>
- Knepper WA (ed) (1962) *Agglomeration*. Interscience Publishers, Geneva
- Korzani MG, Galindo-Torres SA, Scheuermann A, Williams DJ (2018) SPH approach for simulating hydro-mechanical processes with large deformations and variable permeabilities. *Acta Geotech* 13(2):303–316
- Kou B, Cao Y, Li J, Xia C, Li Z, Dong H, Zhang A, Zhang J, Kob W, Wang Y (2017) Granular materials flow like complex fluids. *Nature* 551(7680):360
- Lagrée PY, Staron L, Popinet S (2011) The granular column collapse as a continuum: validity of a two-dimensional Navier–Stokes model with a $\mu(I)$ -rheology. *J Fluid Mech* 686:378–408
- Liu GR, Liu MB (2003) *Smoothed particle hydrodynamics: a meshfree particle method*. World Scientific, Singapore
- Mao Z, Liu GR, Dong X (2017) A comprehensive study on the parameters setting in smoothed particle hydrodynamics (SPH) method applied to hydrodynamics problems. *Comput Geotech* 92:77–95
- Marrone S, Antuono M, Colagrossi A, Colicchio G, Le Touzé D, Graziani G (2011) δ -SPH model for simulating violent impact flows. *Comput Methods Appl Mech Eng* 200(13–16):1526–1542
- MiDi GDR (2004) On dense granular flows. *Eur Phys J E* 14(4):341–365
- Minatti L, Paris E (2015) A SPH model for the simulation of free surface granular flows in a dense regime. *Appl Math Model* 39(1):363–382
- Mitarai N, Nori F (2006) Wet granular materials. *Adv Phys* 55(1–2):1–45
- Monaghan JJ (1994) Simulating free surface flows with SPH. *J Comput Phys* 110(2):399–406
- Monaghan JJ (2000) SPH without a tensile instability. *J Comput Phys* 159(2):290–311
- Morris JP, Fox PJ, Zhu Y (1997) Modeling low Reynolds number incompressible flows using SPH. *J Comput Phys* 136(1):214–226
- Neto AHF, Borja RI (2018) Continuum hydrodynamics of dry granular flows employing multiplicative elastoplasticity. *Acta Geotech* 13(5):1027–1040
- Nguyen CT, Nguyen CT, Bui HH, Nguyen GD, Fukagawa R (2017) A new SPH-based approach to simulation of granular flows using viscous damping and stress regularisation. *Landslides* 14(1):69–81
- Peng C, Guo X, Wu W, Wang Y (2016) Unified modelling of granular media with smoothed particle hydrodynamics. *Acta Geotech* 11(6):1231–1247
- Pouliquen O, Forterre Y (2002) Friction law for dense granular flows: application to the motion of a mass down a rough inclined plane. *J Fluid Mech* 453:133–151
- Richefeu V, El Youssoufi MS, Radjai F (2006) Shear strength properties of wet granular materials. *Phys Rev E* 73(5):051304
- Richefeu V, El Youssoufi MS, Peyroux R, Radjai F (2008) A model of capillary cohesion for numerical simulations of 3D polydisperse granular media. *Int J Numer Anal Methods Geomech* 32(11):1365–1383

38. Rognon PG, Roux JN, Naaim M, Chevoir F (2008) Dense flows of cohesive granular materials. *J Fluid Mech* 596:21–47
39. Samadani A, Kudrolli A (2001) Angle of repose and segregation in cohesive granular matter. *Phys Rev E* 64(5):051301
40. Silbert LE, Ertas D, Grest GS, Halsey TC, Levine D, Plimpton SJ (2001) Granular flow down an inclined plane: Bagnold scaling and rheology. *Phys Rev E* 64(5):051302
41. Staron L, Hinch EJ (2005) Study of the collapse of granular columns using two-dimensional discrete-grain simulation. *J Fluid Mech* 545:1–27
42. Szewc K (2017) Smoothed particle hydrodynamics modeling of granular column collapse. *Granul Matter* 19(1):3
43. Wang JP, Gallo E, François B, Gabrieli F, Lambert P (2017) Capillary force and rupture of funicular liquid bridges between three spherical bodies. *Powder Technol* 305:89–98
44. Wang G, Riaz A, Balachandran B (2017) Computational studies on interactions between robot leg and deformable terrain. *Proc Eng* 199:2439–2444

Publisher's Note Springer Nature remains neutral with regard to jurisdictional claims in published maps and institutional affiliations.